Available online at www.sciencedirect.com
SCIENCE DIRECT
Journal of Nuclear Materials 350 (2006) 40–46
journal of nuclear materials
www.elsevier.com/locate/jnucmat

Analysis for hydrogen particle balance of plasma-wall system in the large helical device

M. Kobayashi [a,*], J. Miyazawa [a], S. Masuzaki [a], Y. Igitkhanov [b], R. Sakamoto [a], N. Ashikawa [a], T. Morisaki [a], N. Ohyabu [a], H. Yamada [a], H. Funaba [a], A. Komori [a], O. Motojima [a], the LHD experimental group

[a] *National Institute for Fusion Science, Oroshi-cho 322-6, Toki 509-5292, Japan*
[b] *Max-Planck-Institut fur Plasmaphysik, Teilinstitut Greifswald, Euratom Association, 17491 Greifswald, Germany*

Received 7 June 2004; accepted 12 November 2005

Abstract

The hydrogen particle balance of the plasma-wall system in the large helical device (LHD) is analyzed, using a zero dimensional model for plasma particles, neutrals in vessel and hydrogen inventory in wall. Based on the measurement of neutral gas pressure, plasma density and the pumping speed of the cryo-pumping system, it is found that the hydrogen retained in the wall desorbes with short and long time constant. The short term desorption is of order of 10^{21} atoms with a time constant of a few minutes, which is much smaller than the wall pumping for one shot, 10^{22} atoms. In a long time scale of about one experimental day, the wall absorbs significantly large amounts of hydrogen, up to 10^{24} atoms. One of the possible reasons for the large wall pumping is a carbon deposition layer on the first wall surface. The effect of hydrogen retention on density control is also discussed.

PACS: 34.00; 52.01.A; 89.02

1. Introduction

In this paper, we investigate the hydrogen particle balance of the plasma-wall system in the large helical device (LHD). Particle balance analysis is important in terms of plasma/impurity density control as well as tritium inventory control in plasma facing components in a fusion reactor. The physical processes governing the balance are: (1) absorption/desorption rate of neutrals into/from the wall (wall pumping capability), (2) location of recycling/sputtering of fuel neutrals/impurities and (3) transport of the fuel neutrals/sputtered impurities in the plasma. The third process, which determines the impurity deposition pattern on the wall, is closely related to the first process because the wall retention capability is considerably dependent on the composition of the materials. The second one is a strong function of the geometry of the divertor components for plasma flux and of the first wall for neutral

* Corresponding author.
E-mail address: masahiro@nifs.ac.jp (M. Kobayashi).

0022-3115/$ - see front matter
doi:10.1016/j.jnucmat.2005.11.016

charge exchange (CX) flux. An understanding of the overall physics thus involves the edge transport of plasma and neutrals as well as the material physics of the wall. There have been a number of studies carried out in this field [1–3]. For example, the results of Ref. [2] indicate the difference in wall pumping capability depending on the wall material selection, while Ref. [3] analyzed the importance of CX flux for the wall pumping. The particle balance in LHD was also analyzed in a few articles in the last several years [4–6], where Refs. [4,5] investigated hydrogen particle balance with all plasma facing components being stainless steel. Since the third experimental campaign in FY 1999, however, graphite tiles have been installed at the divertor leg region, which will strongly affect the plasma-wall interaction processes.

The purpose of this paper is to analyze the hydrogen particle balance in LHD with the full installation of graphite tiles at the divertor region. In Section 2, the experimental details including the wall surface condition are described. In Section 3, the particle balance based on a zero dimensional model is studied. In Section 4, the time constant/amount of the short/long term wall retention are estimated. Also the effect of the wall inventory on the density control is discussed. Section 5 gives a summary of the discussions.

2. Experimental set-up

2.1. Pumps and pressure gauges

The vacuum vessel of LHD is made of SUS 316L, which is water-cooled to around room temperature during operation. The surface area of the vessel, including the ports, is about 700 m^2, half of which is directly facing to plasma. The volume inside the vessel of 210 m^3 is evacuated by a cryo-pumping system (in total 18 cryo-pumps), which provide an effective pumping speed of 700 m^3/s. The plasma volume is about 30 m^3. The divertor is made of graphite armor tiles which have an area of 30 m^2.

The neutral gas pressure is measured with a cold cathode (CC) gauge, an ionization gauge and a fast ionization gauge (ASDEX gauge [7]), that are located at the pumping duct entrance, behind the cryo-pump system and in the vacuum vessel, respectively. The time constants for the gauges are 35 ms for the CC gauge and 1 ms for the ASDEX gauge. The ionization gauge monitors the gas pressure behind the cryo-pump system every 5 s, which is used for estimating the long term evolution of the particle balance. The external particle (hydrogen) fuelling in the present experiments are gas puff fueling of $\sim 10^{23}$ atoms/s, pellet injection $\sim 10^{21}$ atoms/s and neutral beam injection (NBI) $\sim 10^{20}$ atoms/s, respectively, while the pumping speed of the cryo-pump corresponds to 10^{21} atoms/s. In the present experiments, the particle balance is studied at high density operation, $\bar{n}_e \geqslant 8 \times 10^{19}$ m^{-3}.

2.2. Status of the wall surface

The wall pumping capability and the desorption time constant are strongly dependent on the wall surface composition. According to the material probe study [8,9], a substantial amount of carbon is considered to be deposited on the first wall surface. It showed that at the upper (#3) and bottom (#2) first wall and inner private region (#1) (Fig. 1) the deposition layer was 5–10 nm, on the other hand, at the outer private region (#4) and the port (#5) it was more than 50 nm. The difference of the thickness is probably attributed to the plasma flux intensity profile on the surface, i.e., at the outer divertor and the port which are remote from plasma the deposited carbon can accumulate without significant sputtering by plasma exposure.

During the experimental campaign of several months, boronization has been conducted from time to time, and it provides boron films on the vessel wall surface with a thickness of typically a few tens of nm [10]. Although the boronization is done for gettering oxygen, it has been found that the film also enlarges the hydrogen absorption

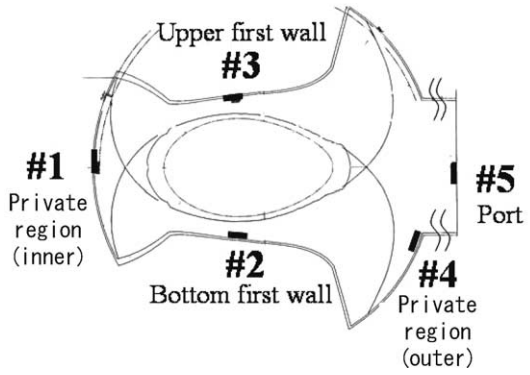

Fig. 1. Schematic of the LHD cross-section. The locations of the material probes in Refs. [8,9], at toroidal section 7, are indicated by black marks (#1–5). The distance between the port (#5) and the outer X point is about 1.5 m.

capacity by 5 times compared to pure stainless steel [11]. But the coverage of the boron film is recently estimated at around 30% of the vessel wall, so that for the present analysis we will neglect the effect of the boronization on the particle balance.

The effects of the carbon layer on the particle balance will be discussed in the following sections.

3. Particle balance analysis

The model used in the present analysis is a 0 dimensional one, which divides the system into plasma, wall and volume between wall and plasma (this region is rather large in LHD compared to other devices, i.e., plasma volume of 30 m^3 and vessel volume of 210 m^3). N_p, N_w and N_n denote the particle inventory in the plasma, of the neutrals in the wall and in the vessel, respectively. From particle conservation, one can simply get the relation,

$$(N_w - N_{w0}) + N_n + N_p = \int_{t=0}^{t} (\Gamma_{in} - \Gamma_{out})dt, \qquad (1)$$

where N_{w0}, Γ_{in} and Γ_{out} are the initial wall inventories at $t = 0$, particle input (fuelling by gas puff, pellet, NBI) and pumping out by cryo-pump, respectively.

The time traces of a typical plasma discharge in LHD are shown in Fig. 2. As a wall conditioning, the boronization followed by the He glow discharge of 3 h was conducted before this experimental day. The density is gradually ramped up by gas puffing in two steps up to 8×10^{19} m^{-3} at $t = 1.2$ s, after which the gas puff is turned-off, being followed by a slight density decrease down to 6×10^{19} m^{-3}. Plotted in Fig. 2(b) are the integrated gas puffed particles, the particles pumped by the wall calculated by Eq. (1) and by the cryo-pump. During the strong gas puff phase at $t = 1$–1.2 s, there exists strong wall pumping, $\sim 5 \times 10^{22}$ atoms/s, as shown in the figure, while after turning off the gas puff the wall inventory keeps almost constant value. This indicates a significant change of the wall pumping characteristic due to the gas puff turn-on/off. The similar behaviour was found in Tore Supra [12]. It was discussed as being due to the broadening of the divertor flux profile, which causes additional wall pumping by bringing particles to the area that are not exposed to the plasma when the gas puff is turned-off [12]. Concerning the divertor flux profile in the present experiments, it is found that near the gas puff valve, the particle flux becomes broad with a reduced averaged flux, while away from the valve the shape of the flux profile scarcely changes. At the moment the resulting effect of the divertor flux change on the wall pumping is not yet identified. On the other hand, the CX flux to the first wall is estimated at about 33% of the gas puff (Appendix A). This roughly corresponds to the wall pumping during the gas puff phase, i.e., 10^{23} atoms $\times 0.33 \sim 3 \times 10^{22}$ atoms. Therefore, if the first wall is capable of a wall pumping for the CX flux, it can be a reason for the strong wall pumping during the gas puff phase.

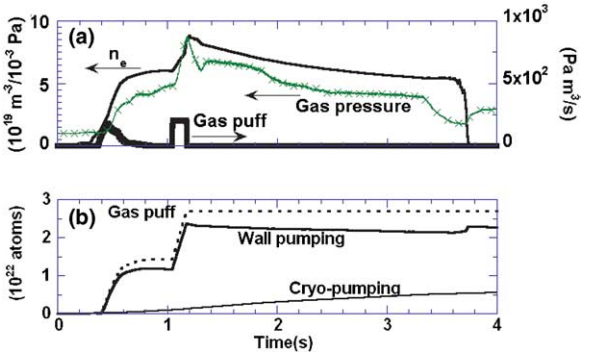

Fig. 2. Time traces of (a) line averaged plasma density, neutral pressure (measured at the pumping duct with the CC gauge) and gas puff, (b) time integrated particle numbers from gas puffing, wall pumping and cryo-pumping, respectively.

From this analysis, it is found that 80% of the gas-fueled particles are pumped by the wall and the rest (20%) by the cryo-pump. The fuelling efficiency of gas puffing is about 10%.

4. Hydrogen retention in wall

4.1. Short term retention

In LHD, the discharges with a duration of several seconds are repeated with about 3 min intervals. Plotted in Fig. 3 is the pumped atoms by the cryo-pumps during and after the discharges as a function of the total divertor particle flux, which is obtained by time-integrating the ion saturation current of the probes embedded in the divertor plates. The amount of pumped particles are almost proportional to the divertor flux, which also scales linearly with plasma density. Because of the high neutral pressure during the discharges, the amount of pumped particles is about 3 times greater than that during the intervals. These particles are categorized being retained for a short term with a time constant of a few minutes, and are considered to be retained in the wall as a solute state.

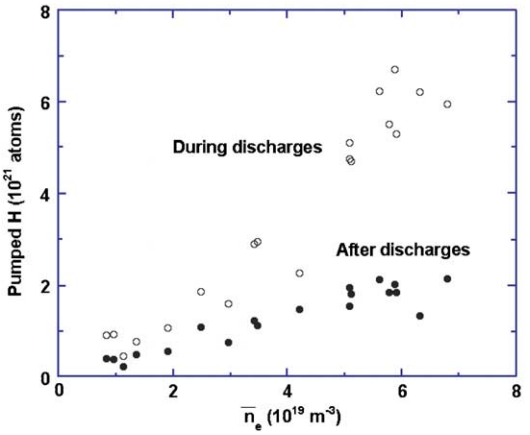

Fig. 3. Pumped hydrogen during (○) and after (●) discharges as a function of total divertor flux during discharges. The divertor flux scales almost linearly with the line averaged density. As the divertor flux increases from 1×10^{23} to 5×10^{23} ions/m^2, the line averaged density changes from 2×10^{19} to 6×10^{19} m^{-3}.

The effect of the hydrogen retained in the wall on density control is often observed. Fig. 4 shows the line averaged plasma density and the amount of gas-fueled particles for a sequence of discharges. One sees that while keeping the density constant, the required gas puffing gradually decreases, indicating an increase of the hydrogen emission from the wall. Finally, at #53584 the same density level, $\bar{n}_e \sim 6\times10^{19}$ m^{-3}, is obtained even though the puff is turned-off. It should be kept in mind, however, that this does not indicate wall saturation because if the puff is kept turned-on, the wall continues to absorb the neutrals, as shown in Fig. 8, with increased plasma density.

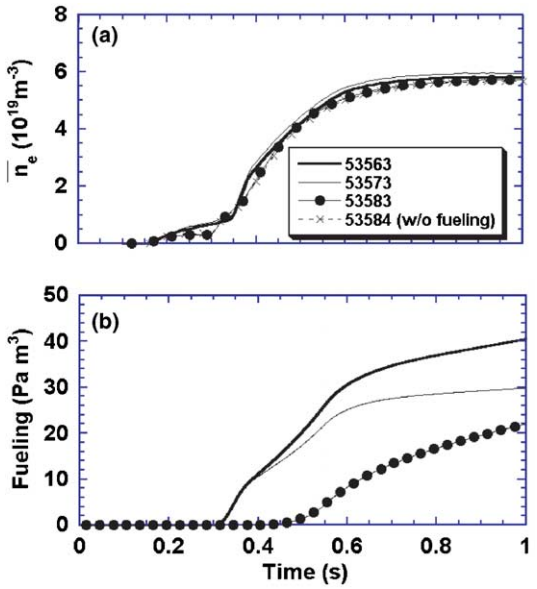

Fig. 4. Time traces of (a) line averaged plasma density and (b) the amount of gas puff for four successive discharges. While keeping the same plasma density, the required gas puff gradually decreases, indicating an increase of the wall inventory.

The discharge has been produced without gas puffing for several consecutive shots. The evolutions of the density and the removed hydrogen from the wall, which is calculated by Eq. (1) are plotted in Fig. 5. The removed hydrogen is sum of the desorption during the discharge and the interval. The depletion of hydrogen during the discharges due to plasma/CX flux bombardment was found to be considerably higher by a factor of 2–5 than that during the intervals. After five shots, the density reaches an almost constant value around $\bar{n}_e = 1\times10^{19}$ m^{-3}, indicating that the particle balance in the plasma-wall system has been brought to an equilibrium state. Indeed, after the sequence the same amount of gas puff as #53563 is required to reach $\bar{n}_e \sim 6\times10^{19}$ m^{-3}. In the sequence of 8 shots, the total amount of depleted hydrogen (sum of the 8 shots) is $\sim1\times10^{22}$ atoms, which corresponds to the wall pumping in one shot, as shown in Fig. 2. It is considered that these particles are retained in the wall in the rather shallow region (probably as a solute state) and not strongly trapped in the carbon layer, so that via bombardment of plasma or CX flux they are released and affect the plasma density.

4.2. Desorption rate of hydrogen retained in wall

After discharge termination, the rate of desorbed hydrogen from the wall can be calculated as,

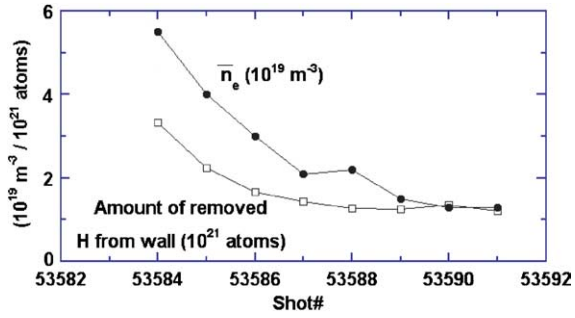

Fig. 5. Plasma density (●) and removed hydrogens (□) from the wall by the cryo-pump during the sequence of no-puff discharges.

$$\frac{\partial N_w}{\partial t} = -\frac{N_w}{\tau_w} = -\frac{\partial N_n}{\partial t} - P_0 \times S_p, \quad (2)$$

where P_0 and S_p are the neutral pressure and pumping speed, respectively. The result is plotted in Fig. 6, with a logarithmic scale together with the traces of plasma density and neutral pressure. Just after the plasma termination, the desorption has a time constant of $\tau_w \sim 0.1$ s, followed by the slower desorption of $\tau_w \sim 3$ s. The amount of the desorbed hydrogen in the fast phase is $\sim 10^{20}$ atoms, which is one order smaller than that of the slow desorption, $\sim 10^{21}$ atoms. Similar behaviour was also reported in Ref. [4], although the time constants were different from the present ones.

The fast time constant could be attributed to a release of over-saturated hydrogen by dynamic retention during the discharge, as has been observed in tokamaks [14]. As for the slow time constant, on the other hand, this almost corresponds to the time needed for the hydrogen to diffuse out of the carbon layer, if one takes $D_H \sim 10^{-17}$ m^2/s [12] with a penetration depth of $\sim$10 nm for the edge plasma temperature of LHD.

The slow time constant was found to increase as the edge temperature increases. Plotted in Fig. 7 is the dependence of the slow τ_w on the electron temperature at $\rho = 1.0$, where ρ is a normalized minor radius at the last closed flux surface. If we assume that the impinging energy of plasma particles onto the divertor tiles $\sim 3T_e$ by sheath acceleration, the penetration depth increases with the edge T_e. Provided also $T_i \propto T_e$, the penetration depth of the CX neutral flux to the first wall increases as well for high T_e. The tendency is thus consistent with the diffusion model for the desorption rate, i.e., the deeper depth makes τ_w longer.

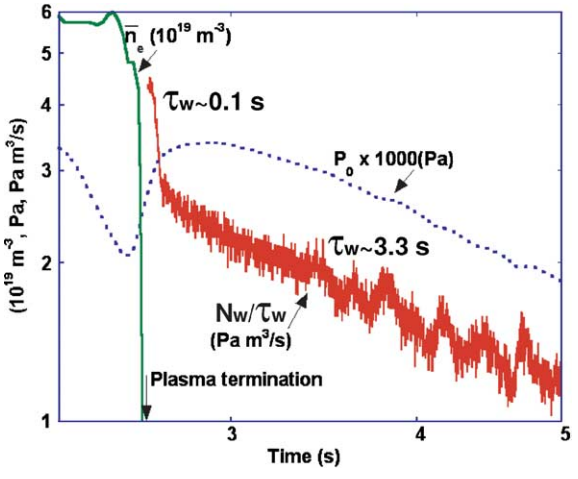

Fig. 6. Desorption rate, N_w/τ_w, just after the discharge termination calculated by Eq. (2), together with neutral gas pressure and plasma density. In the logarithmic plot, it is found that there are two different time constants for the desorption rate, $\tau_w \sim 0.1$ and 3.3 s.

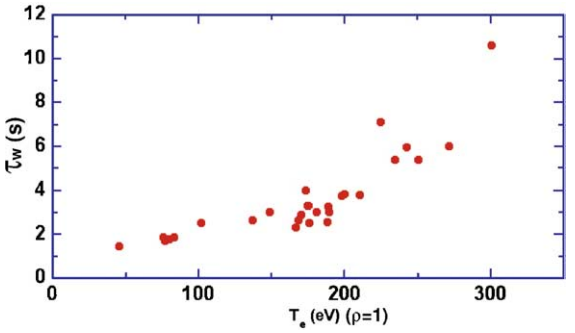

Fig. 7. Dependence of the slow time constant, τ_w, on the edge electron temperature at $\rho = 1$. ρ is a normalized minor radius at the last closed flux surface. The temperature is time-averaged over the flat top of the plasma density.

4.3. Long term retention

Compared to the wall pumping in one shot, $\sim 2 \times 10^{22}$ atoms as shown in Fig. 2, the short term retention is much smaller, $\sim 2 \times 10^{21}$ atoms, and it thus means that on the order of 10^{22} particles are accumulated continuously in the course of the discharge. An example of the time evolution of the hydrogen inventory over a long time scale ($\sim$one experimental day) is shown in Fig. 8, where the particle input (by puff and pellet) as well as the pumped out particles are plotted. In this plot one sees that the wall absorbs in total on the order of 10^{24} particles without saturation at the end of the day, i.e., 4×10^{21} atoms/m^2. This is significantly larger than the long term hydrogen retention, $\sim 5 \times 10^{21}$ H, obtained in Ref. [4], where the graphite divertor tiles were not yet installed. The number is apparently not realistic for a stainless steel wall, e.g., the TdeV tokamak with 94% of first wall being made of SUS316 reached wall saturation at 5.6×10^{19} H/m^2 [2].

A possible reason for the large hydrogen inventory is the carbon deposition layer on the first wall, as mentioned in Section 2.2, which presumably covers a substantial portion of the wall surface. It is also noted that during the discharges the first wall is kept at a rather low temperature (<370 K), which significantly increases the hydrogen retention.

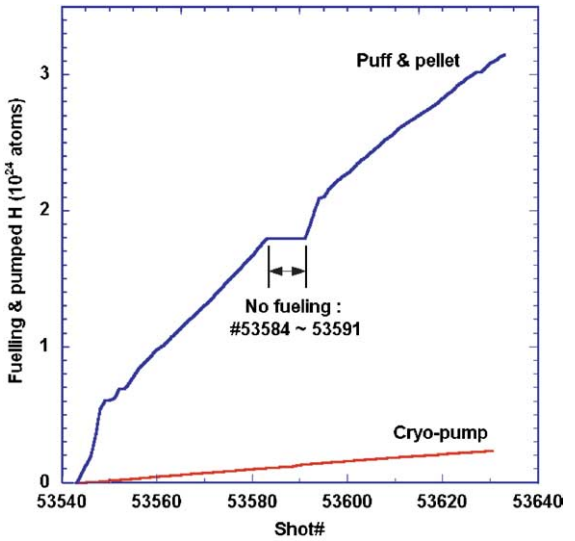

Fig. 8. Time evolution of injected (by puff and pellet) and pumped hydrogen during one experimental day. The most of the hydrogen is found to remain in the vacuum vessel. Total wall inventory at the end of the day amounts to $\sim 10^{24}$ atoms.

Analytical estimations of the CX flux to the first wall (Appendix A) give $\sim 10^{22}$ atoms/s, which is 30% of the puffed particles. The material probe measurement of the CX flux to the first wall also indicates the same order of fluence [13]. From this estimation, it is considered that the CX implantation of neutrals onto the first wall with the carbon deposition layer of several tens nm thickness is a possible candidate for the retention process other than the divertor plate retention.

The graphite tiles of the divertor plates, which are water-cooled to keep the temperature below 600 K, also can be a large reservoir of hydrogen because of their low temperature.

5. Summary

The hydrogen particle balance of the plasma-wall system in LHD has been analyzed using a simple zero dimensional model. We have found,

1. For the typical discharge in LHD with $\bar{n}_e \sim 8 \times 10^{19}\ m^{-3}$, 80% of puffed particles (2×10^{22} atoms) are pumped by the wall and 20% (5×10^{21} atoms) are pumped by the cryo-pump system. The fuelling efficiency is $\sim$10%.
2. The short term retention during one discharge sequence, which is released from the wall during the 3 min interval, is 2×10^{21} atoms. It is one order smaller than the wall pumping in one shot.
3. The effect of the hydrogen retention on the plasma density is observed. The wall retention, which directly affects the plasma density, is found to be 2×10^{22} atoms. They are considered to be retained in the shallow regions of the wall as a solute state. Consequently, via plasma/CX flux bombardment they are released from the wall and affect the plasma density.
4. The wall continues to absorb hydrogen during one experimental day without showing saturation. It amounts to $\sim 10^{24}$ atoms, 4×10^{21} atoms/m^2. Possible reasons for the large amount of wall retention are, (a) the carbon deposition layer on substantial parts of the first wall with a thickness of 5 to several tens of nm, (b) considerably high CX fluence to the first wall $\sim 10^{22}$ H/s, (c) the low wall temperature $\sim < 370$ K, (d) the low temperature of the divertor plate made of graphite tiles $\sim$600 K.
5. The hydrogen desorption after discharge termination has two time constants, $\tau_w \sim 0.1$ s and several seconds. The latter time constant becomes large as the edge T_e increases. The slow τ_w is consistent with an estimation of the desorption time of hydrogen from a carbon layer based on a diffusion model.

Acknowledgements

The authors are grateful to Dr H Takenaga, Dr N Asakura and Professor A Sagara for their fruitful discussions.

Appendix A. Estimation of CX flux to the first wall

For simplicity, assume a slab geometry for plasma and wall surfaces, where a neutral gas occupies the space in-between them. For neutrals flying towards the plasma, the probability of being reflected back to the wall after the first collision (CX) is $\beta/2$, where β is a probability of CX,

$$\beta = \frac{\langle \sigma v \rangle_{CX}}{\langle \sigma v \rangle_{CX} + \langle \sigma v \rangle_{ion}}, \tag{3}$$

here $\langle \sigma v \rangle_{CX}$ and $\langle \sigma v \rangle_{ion}$ are the rate coefficients of CX and ionization, respectively. After the second collision, the reflection probability is then $(\beta/2)^2$. Successively, the probability for the neutrals to be

reflected back to the wall after all collisions, A, is given as,

$$A = \frac{\beta}{2} + \frac{\beta^2}{2} + \frac{\beta^3}{2} + \cdots = \frac{\beta/2}{1-\beta/2}, \tag{4}$$

which is called the albedo. This is also expressed as,

$$A = \frac{1-k}{1+k}, \quad k = \frac{\langle\sigma v\rangle_{\text{ion}}}{\langle\sigma v\rangle_{\text{CX}} + \langle\sigma v\rangle_{\text{ion}}}. \tag{5}$$

Using A, the CX flux to the first wall, j_0^+, is given by $j_0^+ = Aj_0^-$, where j_0^- is the total neutral flux towards plasma, given as,

$$j_0^- = \int_{-\infty}^{0} v f_{\text{M}}(v)\mathrm{d}v = \frac{1}{2} \times \frac{1}{4} n_{\text{a}} \bar{v}_{\text{a}}, \tag{6}$$

here $\bar{v}_{\text{a}} = \sqrt{8T_{\text{a}}/m_{\text{a}}\pi}$ with n_{a}, T_{a} and m_{a} being the atom density, atom temperature and mass of an atom in the vessel, respectively. In a equilibrium state, this flux is equal to $\frac{1}{2} \times 2 \times \frac{1}{4} n_{\text{m}} \bar{v}_{\text{m}}$, which is a molecule flux in the pressure gauge plenum where $\bar{v}_{\text{m}} = \sqrt{8T_{\text{m}}/m_{\text{m}}\pi}$, with n_{m}, T_{m} and m_{m} being the molecule density, molecule temperature and mass of a molecule, respectively. That is,

$$j_0^- = \frac{1}{2} \times \frac{1}{4} n_{\text{a}} \bar{v}_{\text{a}} = \frac{1}{2} \times 2 \times \frac{1}{4} n_{\text{m}} \bar{v}_{\text{m}}. \tag{7}$$

For T_{m} of room temperature $\bar{v}_{\text{m}} \approx 1.9 \times 10^3$ m/s, and from the measurement of the pressure gauge $n_{\text{m}} = p_{\text{m}}/(k_{\text{B}} T_{\text{m}}) \approx 2 \times 10^{17}\ \text{m}^{-3}$ with a typical gas pressure of $p_{\text{m}} \sim 10^{-3}$ Pa in LHD. Thus the fluence of neutrals towards the plasma is,

$$\Gamma_0^- = j_0^- S_{\text{wall}} \approx 3 \times 10^{22}\ \text{atoms/s}, \tag{8}$$

where S_{wall} is the surface area of the first wall facing to the plasma ($\sim$300 m^2). For the edge plasma with $T < 100$ eV, $k \approx 1/2$, so that $A \approx 1/3$. It then gives the CX fluence to the first wall,

$$\Gamma_0^+ = A\Gamma_0^- \approx 10^{22}\ \text{atoms/s}. \tag{9}$$

References

[1] H. Takenaga, A. Sakasai, H. Kubo, N. Asakura, M.J. Schaffer, T.W. Petrie, M.A. Mahdavi, D.R. Baker, S.L. Allen, G.D. Porter, T.D. Rognlien, M.E. Rensink, D.P. Stotler, C.F.F. Karney, Nucl. Fusion 41 (2001) 1777.

[2] R. Maingi, B. Terreault, G. Haas, G.L. Jackson, W. Zuzak, P.K. Mioduszewski, M.A. Mahdavi, M.R. Wade, S. Chiu, M.J. Schaffer, J.T. Hogan, C.C. Klepper, J. Nucl. Mater. 241–243 (1997) 672.

[3] P.K. Mioduszewski, J.T. Hogan, L.W. Owen, R. Maingi, D.K. Lee, D.L. Hillis, C.C. Klepper, M.M. Menon, C.E. Thomas, T. Uckan, M.R. Wade, M. Chatelier, C. Grisolia, Ph. Ghendrih, A. Grosman, T. Hutter, T. Loarer, B. Pegourie, M.A. Mahdavi, M. Schaffer, J. Nucl. Mater. 220–222 (1995) 91.

[4] H. Suzuki, N. Ohyabu, A. Komori, O. Motojimathe LHD experimental group, J. Plasma Fusion Res. 3 (2000) 250.

[5] Y. Hirooka, S. Masuzaki, H. Suzuki, T. Kenmotsu, T. Kawamura, J. Nucl. Mater. 290–293 (2001) 423.

[6] H. Suzuki, N. Ohyabu, A. Komori, T. Morisaki, S. Masuzaki, J. Miyazawa, R. Sakamoto, M. Shoji, M. Goto, S. Morita, Y. Kubota, O. Motojima, the LHD experimental group, J. Nucl. Mater. 313–316 (2003) 297.

[7] G. Haas, J. Gernhardt, M. Keilhacker, E.B. Meserveythe ASDEX team, J. Nucl. Mater. 121 (1984) 151.

[8] T. Hino, Y. Nobuta, Y. Yamauchi, Y. Hirohata, A. Sagara, S. Masuzaki, N. Inoue, N. Noda, O. Motojima, the LHD experimental group, J. Nucl. Mater. 313–316 (2003) 167.

[9] Y. Nobuta, Y. Yamauchi, Y. Hirohata, T. Hino, A. Sagara, S. Masuzaki, N. Ashikawa, N. Noda, O. Motojima, the LHD experimental group, J. Nucl. Mater. 329–333 (2004) 800.

[10] K. Nishimura, N. Ashikawa, S. Masuzaki, J. Miyazawa, A. Sagara, M. Goto, B.J. Peterson, A. Komori, N. Noda, K. Ida, O. Kaneko, K. Kawahata, T. Kobuchi, S. Kubo, S. Morita, M. Osakabe, S. Sakakibara, R. Sakamoto, K. Sato, T. Shimozuma, Y. Takeiri, K. Tanaka, O. Motojimathe LHD experimental group, J. Nucl. Mater. 337–339 (2005) 431.

[11] K. Tsuzuki, M. Natsir, N. Inoue, A. Sagara, N. Noda, O. Motojima, T. Mochizuki, T. Hino, T. Yamashina, J. Nucl. Mater. 241–243 (1997) 1055.

[12] M. Sugihara, G. Federici, C. Grisolia, P. Ghendrih, J.T. Hogan, G. Janeschitz, G. Pacher, D.E. Post, J. Nucl. Mater. 266–269 (1999) 691.

[13] M. Miyamoto et al., 'Erosion of plasma facing materials by charge exchange neutrals in LHD', 3rd workshop on PWI issues in LHD, 6th June 2005, NIFS Japan.

[14] V. Phillips, E. Vietzke, M. Erdweg, F. Waelbroeck, J. Nucl. Mater. 162–164 (1989) 520.